Development of an Experimental Protocol to Study the Neural Control of Force and Impedance in Wrist Movements with Robotics and fMRI

Kristin Schmidt, Bastien Berret, and Fabrizio Sergi

***Abstract*— Robotic exoskeletons have emerged as beneficial tools in the field of rehabilitation, yet their full potential is impeded by our limited knowledge of the neural control of movements during human-robot interaction. To personalize exoskeleton protocols and improve individuals' motor recovery, we must advance our understanding of how the brain commands movements in physical interaction tasks. However, interpreting the neural function associated with these movements is complex due to the simultaneous expression of at least two control policies: force and impedance control. This hinders our ability to isolate these control mechanisms and pinpoint their neural origins. In this study, we evaluate the capacity of external force fields to decouple the expression of force and impedance in a wrist-pointing task, a necessary step in isolating their neural substrates via neuroimaging.**

We first conducted simulations using a neuromuscular model to examine how both force and impedance commands are updated when participants are asked to perform reaching movements in the presence of an external force field. Then, we recruited seven participants to perform a wrist-pointing task with the MR-SoftWrist, an MRI-compatible wrist robot. The task included four different force field conditions – no force, positive constant force, negative constant force, and divergent force, each carefully selected to decouple expression of force and impedance control. Furthermore, we evaluated the efficacy of our proposed conditions for a neuroimaging experiment through simulations of neural activity. We show that these force fields elicit distinct and predictable torque and stiffness expression, laying the groundwork for reliably identifying their associated neural activity in a future neuroimaging study.

I. INTRODUCTION

Force and impedance control represent fundamental control strategies enabling skillful human movement. Force control dominates in predictable and stable tasks, where the Central Nervous System (CNS) builds an internal model of appropriate motor commands [1]. In this case, the CNS coordinates the reciprocal activation of muscle pairs to generate desired torques. When faced with unpredictable or unstable environmental dynamics, the CNS also uses impedance control to mitigate disturbances [2], [3]. This involves the modulation of joint stiffness through the simultaneous contraction of agonist and antagonist muscle pairs. The precise regulation of force and impedance is not only essential for everyday motor tasks but also holds significant importance in expanding our knowledge of neuromuscular disorders. Following neural injuries, such as strokes, there is an alteration in the regulation of force and impedance control, often resulting in excessive co-contraction which contributes to motor impairment [4], [5]. There is still a lot that is unknown about the broader effects of these disorders on various motor pathways, limiting our ability to precisely target rehabilitation efforts for restoring neural function.

The role of impedance control has been well established in behavioral tasks with unstable or unpredictable dynamics [2], where the regulation of joint stiffness via co-contraction promotes task stability. However, this simultaneous contraction of agonist and antagonist muscles increases metabolic costs and is often considered a waste of energy in learnable tasks, where there is no clear advantage to regulating joint stiffness. Yet, in wrist movements, impedance control is significant alongside force generation in stable environments [6]. This co-occurrence of force and impedance presents a challenge for isolating their control during a neuroimaging experiment.

To first explore how individuals should regulate both force and impedance control in reaching tasks with stable force fields, we use the Stochastic Optimal Open-Loop Control (SOOC) framework [7]. While most neuromuscular models based on optimal control cannot predict muscle impedance, SOOC was developed to account for both force and impedance control. We adapt SOOC to describe our wrist-pointing task and evaluate how joint torque and stiffness responses vary across a range of cost functions and noise parameters. Then, with insights obtained from the model simulations, we introduce and assess four force field perturbation conditions in an experimental 2-DOF wrist-pointing task to maximally decouple force and impedance control. Subsequently, we utilize the torque and stiffness relationships characterized in the experimental study to simulate neural responses in a virtual neuroimaging experiment. These simulations aim to evaluate the effectiveness of the proposed force field conditions to elicit neural activation that can be correctly ascribed to each of the assumed control policies using a simple general linear model approach. This combination of neuromuscular modeling, behavioral experiments, and simulated neural activity establishes the foundation for a future neuroimaging study, aiming to precisely locate the neural correlates of force and impedance control of the wrist.

II. THEORETICAL FRAMEWORK

To locate the neural origins of co-contraction, one might consider a study design with two types of tasks, such as one with low instability (i.e., a no force task) and one with high instability (i.e., a divergent force task). However, these tasks alone are insufficient to distinguish whether the ensuing neural signal is attributable to the cortical control of muscle co-contraction (i.e., synergistic co-activation

FS (corresponding author - fabs@udel.edu) and KS are with the Human Robotics Laboratory, Departments of Biomedical and Mechanical Engineering, University of Delaware, Newark, DE, 19713 USA. BB is with CIAMS, Université Paris-Saclay, 91405 Orsay, France.

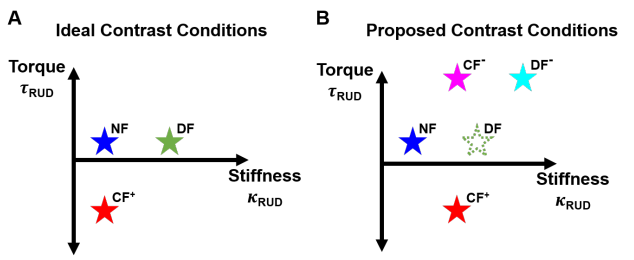

Fig. 1. Hypothesized relationship between torque and stiffness in response to externally applied forces during a wrist-pointing task. (A) In the ideal case, there is no change in stiffness in CF relative to NF, so the contrasts DF-NF and CF-NF control for torque or stiffness, respectively. This is not the case for wrist movements, which motivates our experimental study to evaluate whether our proposed experimental conditions elicit distinct responses. (B) Our experimental task includes the conditions shown on the right with solid stars, and the dotted star for DF was placed for reference.

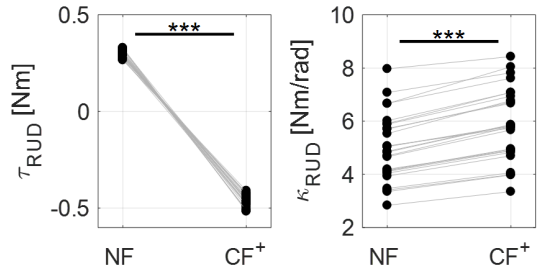

Fig. 2. Optimal SOOC-predicted mean torque and stiffness responses. Each gray line represents a combination of cost function and noise parameters. We tested three levels of cost function weights on final variance ($q_f = \{0.5, 1, 2\}$) and stiffness relative to torque ($\alpha = \{0.5, 1, 2\}$). We show results from signal-dependent noise $d = \{0.2, 0.4, 0.6\}$ and constant noise $\sigma = 0.1$. *** indicates a population difference with $p < 0.001$.

of agonist-antagonist muscle pairs that leads to increased joint impedance), or to separate, independent increases in activation of agonist and antagonist muscles to produce greater forces in the high instability condition. Thus, it is not possible with only these two tasks to determine if there are regions in the brain that contribute to the neural control of co-contraction or if muscle-specific regions are responsible for these commands. Introducing a constant force condition could address this limitation, with the expectation that compensation would primarily result from updates in the internal model based on predicted task dynamics. In an ideal case, the constant force condition would result only in changes in net torque relative to the no force condition, isolating commands specific to agonist force generation (Fig. 1A). However, insights from previous work done in our lab [6] caution against assumptions of negligible impedance control in dynamic wrist movements.

We first investigate how torque and stiffness may co-vary with the magnitude of applied perturbations using a neuromuscular model and decide what experimental conditions are suitable to maximally dissociate them. This approach enhances our ability to isolate and interpret neural commands associated with force generation and impedance control.

A. Predictions Using a Neuromuscular Model

We use the Stochastic Optimal Open-Loop Control (SOOC) framework [7] to probe the relationship between torque and stiffness in both a no force (NF) and constant force (CF) condition. We opted to use the SOOC framework because it is well suited to account for muscle impedance. SOOC predicts optimal feedforward motor commands by minimizing a cost function that penalizes effort and final variance. In this formulation, the main factors that determine optimal torque and stiffness values are the relative weights on final error and stiffness relative to torque. Motor noise is also added to the system and primarily affects the propagation of the covariance. This noise includes both constant (σ) and signal-dependent components (d, proportional to τ). The methods for using this framework are published in [7].

We modeled a single-joint system, representing the wrist, with two degrees of freedom allowing rotation in flexion-extension (FE) and radial-ulnar deviation (RUD). We considered a wrist extension task with either no externally applied forces (NF: $\tau_{FE} = \tau_{RUD} = 0$) or with a constant force applied perpendicular to movement direction (CF: $\tau_{RUD} = 0.6$ Nm). We found that in many cases, including those with low constant noise ($\sigma = 0.1$), the optimal solution is to increase both τ_{RUD} and κ_{RUD} in CF relative to NF (Fig. 2). Since we demonstrate that impedance control is non-negligible in the constant force condition, we must carefully select experimental conditions that allow for contrasts to identify both force and impedance control at the neural level.

B. Task Selection

Because our model results indicate that stiffness may be regulated as a function of applied torque in a CF task, we cannot simply assume a change in torque from the NF task, depicted as a vertical shift in Fig. 1A. Qualitatively, the increase in stiffness would place CF to the right of NF on the torque-stiffness plot, and the response to applied torque would place it above or below NF, depending on the force direction (Fig. 1B). Because the relationship between DF-NF and CF-NF is no longer orthogonal as it was in the ideal case, we cannot conclude that the CF and DF would be placed in significantly different regions without any further information about the selected force fields. Thus, we need to experimentally determine conditions that elicit a distinct torque and stiffness response.

We plan to include the CF condition in two directions (CF^+ and CF^-) to distinguish the neural commands associated with producing torque in any direction and the commands directed to a specific muscle to produce direction-specific torque. We choose the magnitude of the force field to be ± 0.3 Nm, which should be strong enough to yield statistically different results from the NF condition, but not too strong to be overly fatiguing after many trials.

In place of a traditional divergent force condition, we propose a divergent force condition with an offset (DF^-) to act as the high stiffness condition, such that $\tau_{RUD} = k\theta_{RUD} + c$. When $c < 0$, the majority of the workspace is located in a region where the perturbation torque is applied

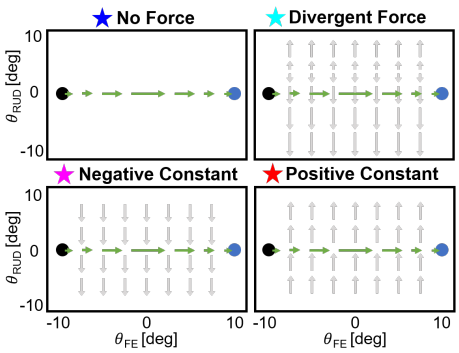

Fig. 3. Proposed experimental force fields. In each task, the goal is to move the cursor from the black target to the blue target in a straight line.

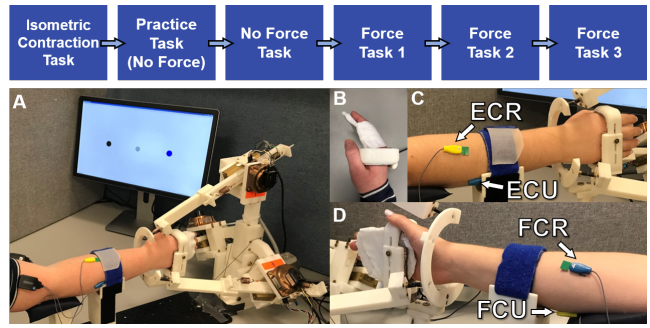

Fig. 4. Top: Experimental task sequence; Bottom: (A) MR-SoftWrist during task performance, (B) top view of device handle, where fingers are secured in a flexed position, (C-D) EMG electrodes placed on four wrist muscles.

down (Fig. 3). This proves advantageous for our study because, with a predictable force direction, we can designate specific muscles as agonists or antagonists, enabling the use of the activation of the pure antagonist muscle [6] as an index of muscle co-contraction for this task. Note that this definition is not possible with a standard divergent force field, such as in [2], because the perturbation direction cannot be predicted. We chose $c = -0.3$ Nm, such that in the straight line trajectory between targets ($\theta_{RUD} = 0$), the force experienced is the same as the CF$^-$ condition. The position-dependent gain k is set as 0.085 Nm/deg, which is strong enough to introduce sufficient instability. Thus, we expect a similar torque response to the CF$^-$ condition and an increase in stiffness resulting from the stiffness necessary to counter both the offset and the added instability of the position-dependent force field (Fig. 1B).

III. BEHAVIORAL EXPERIMENT

A. Experimental Procedure

Seven healthy young adults (3 male, age: 26 ± 3 years, all right-hand dominant) free from neurological or musculoskeletal injury participated in this single-session study. This study was approved by the Institutional Review Board of the University of Delaware, IRB no. 1936400-2.

The experimental protocol is shown in Fig. 4. At the beginning of the session, EMG sensors were placed on the participant's four major wrist muscles: flexor carpi radialis (FCR), flexor carpi ulnaris (FCU), extensor carpi ulnaris (ECU), and extensor carpi radialis (ECR). Sensors were placed on the participant's dominant arm (Fig. 4C-D). We used Delsys Trigno Duo electrodes (sampling frequency: 2148 Hz), and the EMG signal was time-synced to task performance data (sampling frequency: 1000 Hz) via a common analog signal. Electrodes were placed along the muscle belly at the location of the largest agonist muscle contraction. The forearm was prepared for electrode placement by shaving the arm hair and cleaning the skin with alcohol.

EMG activation was first measured during isometric contractions. Participants were cued to apply and hold a torque of 1 Nm for 7 seconds three times in each direction (flexion, extension, radial deviation, and ulnar deviation). This procedure was repeated twice: once in a neutral wrist posture ($\theta_{FE} = \theta_{RUD} = 0$ deg) and again in a flexed posture ($\theta_{FE} = 5$ deg, $\theta_{RUD} = 0$ deg). Agonist muscle contractions were used to confirm correct electrode placement, quantify signal quality, and normalize signals across participants.

In all motor tasks, participants used the MR-SoftWrist (Fig. 4A), an MRI-compatible wrist robot that supports wrist movements in FE and RUD [8]. Participants secured their hand in the robot's handle which clamps around their knuckles without restricting their fingers (Fig. 4B). A small paddle was inserted into the handle to encourage a slightly flexed posture and prevent a power grip [9]. Participants were instructed to focus on performing wrist movements while keeping their fingers as relaxed as possible to minimize coactivation with finger muscles.

Participants controlled a cursor on a monitor by moving the handle in FE and RUD to move the cursor left/right and up/down, respectively. Participants were cued to move the cursor (radius: 1.5 deg) in a straight line between two circular targets (radii: 1.75 deg) located at (±10,0) deg in (FE, RUD). Trial onset was cued by a change in target color from black to blue. Once the participant moved the cursor 1.5 deg laterally toward the target, the cursor was hidden and the force field was initiated, if applicable. The trial ended when the participant passed the lateral position of the target ($\theta_{FE} = \pm 11$ deg) and the robot assisted the user back to the target via a convergent force field (virtual stiffness = 100 Nm/deg). Two forms of feedback were displayed to the user at the end of each trial: speed feedback and position error feedback. Speed feedback was displayed by turning the target red if the movement duration was greater than 500 ms or green if it was less than 200 ms. Otherwise, the target remained black. Error feedback was displayed via a small yellow circle (radius: 1 deg) located directly above or below the target, at the distance of the maximum RUD error during the trial. Both forms of feedback were displayed for 0.5 s after every trial and followed by a random inter-trial interval selected from a normal distribution $\mathcal{N}(0.75, 0.25)$ s, bounded between [0.2, 0.8] s before cueing the next trial.

Participants practiced the task in a transparent (no force) condition to familiarize themselves with the task, understand the displayed feedback, and ask any questions. After familiarization, participants completed four blocks of 200 trials,

with about five minutes of rest in between blocks to minimize muscle fatigue. We chose 200 trials to account for a sufficient number of trials to reach steady-state conditions (first 100 trials) and have enough steady-state trials to provide a sufficient signal-to-noise ratio (last 100 trials). The first block was always an NF task to measure baseline performance, and the next three blocks were presented in a randomized order and included a positive constant force block (CF^+), a negative constant force block (CF^-), and an offset divergent force block (DF^-) (Fig. 3, 4), as described in Section II-B. For participant safety and continuous operation, the divergent force condition was saturated at ± 1 Nm.

B. Data Analysis

Signal-to-noise ratio (SNR) was calculated during the isometric contraction task to confirm electrode placement and quantify signal quality. We defined SNR for each muscle i as

$$SNR_i = \frac{\text{mean}(m_i(t_{ag})) - \text{mean}(m_i(t_{ant}))}{\text{mean}(m_i(t_{ag})) + \text{mean}(m_i(t_{ant}))} \quad (1)$$

where m represents the mean recorded EMG signal during an isometric contraction, and t_{ag} and t_{ant} are the times when i is agonist or antagonist, respectively. This formulation for SNR intuitively shows that a signal for a muscle is +1 if it is active only in its agonist direction or -1 if the muscle is only active in its antagonist direction. An SNR of zero indicates that the muscle is equally active in its expected agonist and antagonist directions. We computed SNR in the FE and RUD directions for each posture.

For trial-by-trial data analysis, trial onset (t_0) was defined as the instant the cursor passed a position threshold of 1.5 deg away from the starting target. Trial end (t_{end}) was defined as the instant the cursor passed a position threshold of 9 deg. To normalize across trials, we defined three key time windows: early, middle, and late trial. The early window starts 150 ms before t_0 and continues until t_0. The middle starts at t_0 and ends when maximum flexion-extension velocity is reached (t_{vmax}), and the late trial starts at t_{vmax} and ends at t_{end}.

Flexion and extension trials were considered separately, and out of each block of 200 trials, we considered only the last 100 trials to remove the transients of learning each force field. EMG signals are bandpass filtered at 30-500 Hz, rectified, and the envelope is taken via a 10 Hz low-pass, zero-shift 4th order Butterworth filter.

1) Muscle Level: As an index of co-contraction, we considered the activity of the pure antagonist [6], that is, the muscle that is antagonistic in both movement direction and perturbation direction (Table I). Accounting for the force of gravity acting on the NF condition, perturbations were applied in the same direction in the NF, CF^-, and DF^- conditions, and thus the activity of the pure antagonist can be directly compared for these conditions.

2) Joint Level: We used the isometric contraction task to estimate muscle-specific scaling factors to compute muscle forces and joint torque and stiffness via a forward dynamics estimation procedure [10]. For each posture tested, we obtained muscle-specific moment arms from OpenSim [11].

TABLE I
PURE ANTAGONIST MUSCLES IN EACH FORCE CONDITION

Force Condition	Flexion Trials	Extension Trials
NF	ECU	FCU
CF^+	ECR	FCR
CF^-	ECU	FCU
DF^-	ECU	FCU

The moment arms were compiled into a Jacobian matrix $\boldsymbol{J}$, where the rows i correspond to a wrist degree of freedom (FE or RUD) and the columns j correspond to a specific muscle, resulting in a 2×4 matrix. Then, EMG measurements m were related to joint torque:

$$\boldsymbol{\tau} = \boldsymbol{JF}, \;\; F_j = \gamma_j m_j + k_j \quad (2)$$

Muscle scaling and offset factors ($\boldsymbol{\gamma}$ and $\boldsymbol{k}$, respectively) were determined by relating measured torques from the F/T sensor to these estimates with a least-squares regression:

$$\boldsymbol{Xz} - \boldsymbol{\tau}_{meas} = \boldsymbol{0}, \;\; \boldsymbol{X} = [\boldsymbol{M}\,\boldsymbol{J}] \quad (3)$$

where $\boldsymbol{z} = [\boldsymbol{\gamma}; \boldsymbol{k}]$ is a 8×1 vector and $\boldsymbol{M}$ is a 2×4 matrix with elements $M_{ij} = J_{ij} m_j$.

Joint stiffness was estimated using the short-range stiffness approximation [12]:

$$\boldsymbol{k}_{SRS} = \frac{a\boldsymbol{F}}{l_0} \quad (4)$$

where a is a dimensionless scaling constant (a = 23.4) [12] and l_0 is the optimal muscle fiber length at maximum activation, as defined in OpenSim [11]. Joint level stiffness was computed as:

$$\boldsymbol{\kappa} = \boldsymbol{J}\,\text{diag}(\boldsymbol{k}_{SRS})\,\boldsymbol{J}^T \quad (5)$$

We also estimated the resulting contributions to torque in the direction of perturbation at the joint level as:

$$u_R = J_{2,FCR} F_{FCR} + J_{2,ECR} F_{ECR} \quad (6)$$

$$u_U = J_{2,FCU} F_{FCU} + J_{2,ECU} F_{ECU} \quad (7)$$

where $J_{2,j}$ is the muscle's RUD moment arm and F_j is the estimated force. These quantities were evaluated to define a compound metric of agonist and antagonist activation, useful for defining co-contraction at the joint level.

C. Statistical Testing

We used the Wilcoxon Signed Rank test to evaluate torque and impedance across the different conditions in the early time window, selected to focus on planned actions rather than online feedback responses. At the muscle level, we used the mean activations of the pure antagonist as a proxy for joint stiffness. At the joint level, we estimated mean κ_{RUD}, τ_{RUD}, u_R, and u_U. To focus on changes induced by each force condition and remove subject-specific biases, the mean in each force condition was subtracted by the mean in NF.

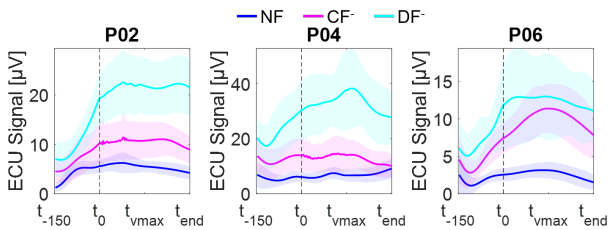

Fig. 5. Subject-level pure antagonist responses of ECU for steady-state, flexion trials for three representative subjects. The bold line represents the mean muscle activity across the group, and the shaded area represents one standard deviation above and below the mean.

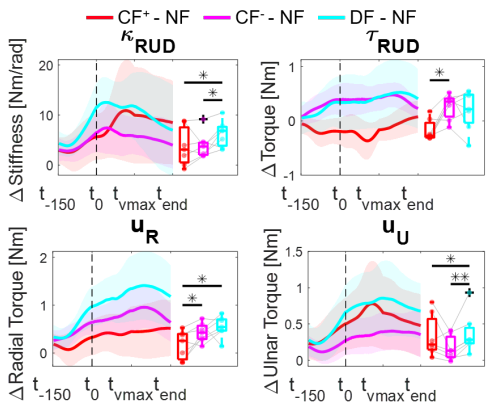

Fig. 6. Group-level torque and stiffness estimates for steady state, flexion trials, normalized by NF activity. The boxplots show the distribution of each subject's mean activity in the early time window ($t_{-150} : t_0$). We tested the significance of median differences with the one-tailed Wilcoxon Signed Rank test, representing $p < 0.05$ with $*$ and $p < 0.01$ with $**$.

D. Results

In flexion trials, where ECU is the pure antagonist in NF, CF$^-$, and DF$^-$, we observe an increase in its mean activity in CF$^-$ and DF compared to NF in all participants. This result is significant at the group-level (CF$^-$-NF: $p = 0.0078$, DF-CF: $p = 0.0078$). The pure antagonist activity (ECU) is shown for three participants in Fig. 5. In extension trials, where FCU is the main pure antagonist, we observe increases in its mean activity from NF to CF$^-$ in 6/7 participants (not significant at the group level at α=0.05: $p = 0.0547$). We also observe significantly greater pure antagonist activity in DF$^-$ compared to CF$^-$ in 6/7 participants ($p = 0.039$).

At the group-level, we find a significant increase in k_{RUD} in the normalized DF$^-$ condition compared to both CF$^+$ ($p = 0.0391$) and CF$^-$ conditions ($p = 0.0156$) in flexion trials (Fig. 6. There are no significant differences in group-level κ_{RUD} in extension trials, but there is a trend of increasing κ_{RUD} from CF$^-$ to DF$^-$ in 6/7 participants. In extension trials, there is a significant increase in τ_{RUD} in the DF$^-$ condition compared to CF$^+$ ($p = 0.0078$).

IV. SIMULATED NEUROIMAGING EXPERIMENT

The ultimate goal of this project is to characterize patterns of torque and stiffness expression such that their neural commands can be maximally decoupled and identified during functional magnetic resonance imaging (fMRI). Here, we use a general linear model approach in a simulated fMRI experiment to examine if our proposed force field conditions are sufficient to distinguish between the neural representations of agonist muscle activation, antagonist activation, and co-activation. To do this, we simulate neural signals based on our experimental results and evaluate if we can differentiate activation associated with each state.

We intend to use a block design, where we will consider all steady-state trials from each condition. We expect the hemodynamic response to remain high for the duration of the block because the blood-oxygen-level-dependent (BOLD) signal that is measured during fMRI is slow to respond (temporal resolution: ∼1-3 seconds) and thus will not have time to decrease between trials. Then, we simply predict mean activation for each experimental condition based on the group-level mean in the early time window during flexion trials from the experimental study. To determine how many steady-state trials are needed, we evaluate study designs with N = 100, 150, or 200 trials.

We defined General Linear Models (GLMs) for regression onto our simulated fMRI data. Our regressors of interest are stiffness (κ_{RUD}), absolute torque ($|\tau_{RUD}|$), and direction-specific torque (u_R and u_U). Here, u_R is the contribution to torque in the radial direction (6), and u_U is the contribution in the ulnar direction (7). The linear dependency between explanatory variables makes the inclusion of all four regressors result in a reduced-rank experimental matrix, so we define two GLMs to fully explain all voxel types:

$$GLM_1 : y = \beta_0 + \beta_1 \cdot \kappa_{RUD} + \beta_2 \cdot |\tau_{RUD}| + \beta_3 \cdot u_R \quad (8)$$

$$GLM_2 : y = \beta_0 + \beta_1 \cdot \kappa_{RUD} + \beta_2 \cdot |\tau_{RUD}| + \beta_4 \cdot u_U \quad (9)$$

To consider all potential representations of κ_{RUD}, $|\tau_{RUD}|$, u_R, and u_U, we define eight voxel types, which respond to κ, $|\tau|$, u_R, u_U, $\kappa + u_R$, $\kappa + u_U$, $\kappa + |\tau|$, or none of these. For each of the simulated voxels, we added zero-mean Gaussian noise with a standard deviation equal to the maximum expected signal for each regressor (SNR=1). Each simulation was run 1,000 times to evaluate how well each model correctly identified each voxel type.

A. Data Analysis

We performed a regression with the simulated neural activity and each GLM to calculate the estimated contribution of each regressor ($\kappa_{RUD}, |\tau_{RUD}|, u_R, u_U$) to the measured signal, known as the β estimates. We considered the bounds on the confidence interval for each β estimate to determine if each regressor is positively or negatively correlated with the simulated neural activity. We calculated the detection rate by considering the number of cases where $\beta > 0$ for the correct voxel types out of the total number of simulations run.

In our approach, no single model can directly explain the signal from all the considered voxel types, due to the reduced-rank problem described earlier. When the explanatory variable for a specific voxel is not directly included in the model, a negative β coefficient is typically estimated, so to effectively combine the information conveyed by the

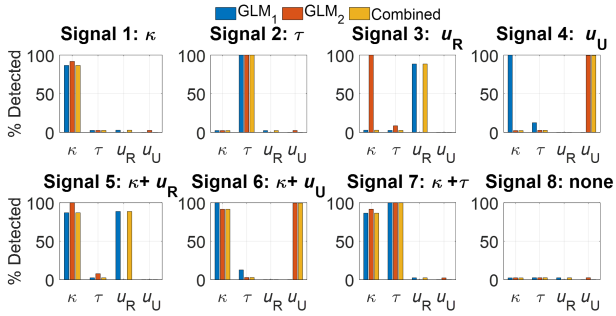

Fig. 7. Detection rate of each state when SNR=1 and N=150.

two GLMs into one model, we started with GLM_1 (8) and examined the β weights estimated for each regressor. If $\beta < 0$, then we used the estimated β weights from GLM_2 (9) for that signal. This combined signal is useful for fMRI analysis, where the true voxel types are not known.

B. Results

When N = 100 trials, we find that across all voxel types, there is a minimum successful detection rate of 70.1% and a maximum false positive detection rate of 2.7%. The success rate improves with the length of each block (N=150: 86.69%, N=200: 94.27%), while the false positive rate remains low (N=150: 2.8%, N=200: 2.69%).

V. DISCUSSION

This study outlines steps in designing a neuroimaging experiment to dissociate the neural substrates of torque and impedance. We designed experimental task conditions to elicit a unique combination of torque and impedance, based on insights from prior work and neuromuscular modeling. Our experimental results reveal unique muscle responses in flexion trials (Fig. 6), while in extension trials, κ_{RUD} showed no significant difference across force conditions. This aligns with prior work that highlights stronger co-contraction effects in wrist flexion movements compared to extension [13]. This suggests that significant differences in co-contraction may only occur in flexion trials under these force conditions. In our fMRI study, we will only include flexion trials and command the robot to return the cursor to the starting position after every trial.

The DF^- condition, unique to this study, proves useful in cases where EMG measurements are noisy. Our primary outcomes of torque and stiffness are estimated via EMG at the joint level, which is susceptible to errors due to variations in normalization and noise levels across EMG electrodes. Defining DF^- with the offset permits us to predict the direction of the applied perturbation, enabling the identification of specific muscles as pure antagonists. This approach allows us to contrast the effects of force conditions within a single muscle, providing an additional metric of co-contraction that is not influenced by normalization errors. In our study, we observed that in the RUD direction, FCR had a much lower SNR (0.1±0.42) on average than all the other muscles (FCU: 0.83±0.21, ECU: 0.68±0.11, ECR: 0.74±0.16). Fortunately, FCR was only the pure antagonist muscle in CF^+ (Table I), so we can still fully evaluate co-contraction via the ranked order of activity of the pure antagonist in NF, CF^-, and DF^-. We observe that the pure antagonist activity was ranked in the expected order of conditions in every participant in flexion trials and 6/7 participants in extension trials, in agreement with our joint level estimation of κ_{RUD} (Fig. 6).

Next, we computed simulations of neural activity and assessed whether these responses could be isolated via general linear models. Our simulations indicate that with this level of noise, at least 150 steady-state trials are needed to obtain results powered to detect all voxel types at the 80% level.

In conclusion, we show that the NF, CF^+, CF^-, and DF^- conditions evoke distinct muscle responses and are well suited for study during fMRI. This represents an important first step in isolating the neural origins of co-contraction, which has numerous implications for better understanding motor control processes and their impact on motor pathways.

REFERENCES

[1] D. M. Wolpert, Z. Ghahramani, and M. I. Jordan, "An Internal Model for Sensorimotor Integration," *Science*, vol. 269, pp. 1880–1882, 3 1995.

[2] E. Burdet, R. Osu, D. W. Franklin, T. E. Milner, and M. Kawato, "The central nervous system stabilizes unstable dynamics by learning optimal impedance," *Nature*, vol. 414, pp. 446–449, 11 2001.

[3] R. Osu, E. Burdet, D. W. Franklin, T. E. Milner, and M. Kawato, "Different Mechanisms Involved in Adaptation to Stable and Unstable Dynamics," *Journal of Neurophysiology*, vol. 90, pp. 3255–3269, 11 2003.

[4] M. L. Latash, "Muscle coactivation: definitions, mechanisms, and functions," *Journal of Neurophysiology*, vol. 120, pp. 88–104, 3 2018.

[5] W. Sheng, S. Li, J. Zhao, Y. Wang, Z. Luo, W. L. A. Lo, M. Ding, C. Wang, and L. Li, "Upper Limbs Muscle Co-contraction Changes Correlated With the Impairment of the Corticospinal Tract in Stroke Survivors: Preliminary Evidence From Electromyography and Motor-Evoked Potential," *Frontiers in Neuroscience*, vol. 16, 6 2022.

[6] A. J. Farrens, K. Schmidt, H. Cohen, and F. Sergi, "Concurrent Contribution of Co-Contraction to Error Reduction During Dynamic Adaptation of the Wrist," *IEEE Transactions on Neural Systems and Rehabilitation Engineering*, vol. 31, pp. 1287–1296, 2023.

[7] B. Berret and F. Jean, "Stochastic optimal open-loop control as a theory of force and impedance planning via muscle co-contraction," *PLoS Computational Biology*, vol. 16, 2 2020.

[8] A. Erwin, M. K. O'Malley, D. Ress, and F. Sergi, "Kinesthetic Feedback during 2DOF Wrist Movements via a Novel MR-Compatible Robot," *IEEE Transactions on Neural Systems and Rehabilitation Engineering*, vol. 25, pp. 1489–1499, 9 2017.

[9] W. L. Popp, O. Lambercy, C. Müller, and R. Gassert, "Effect of Handle Design on Movement Dynamics and Muscle Co-activation in a Wrist Flexion Task," *International Journal of Industrial Ergonomics*, vol. 56, pp. 170–180, 11 2016.

[10] D. R. Smith, C. A. Helm, A. Zonnino, D. J. McGarry, C. L. Johnson, and F. Sergi, "Individual Muscle Force Estimation in the Human Forearm using Multi-Muscle MR Elastography (MM-MRE)," *IEEE Transactions on Biomedical Engineering*, vol. 70, pp. 3206–3215, 11 2023.

[11] K. R. Saul, X. Hu, C. M. Goehler, M. E. Vidt, M. Daly, A. Velisar, and W. M. Murray, "Benchmarking of dynamic simulation predictions in two software platforms using an upper limb musculoskeletal model," *Computer methods in biomechanics and biomedical engineering*, vol. 18, p. 1445, 10 2015.

[12] X. Hu, W. M. Murray, and E. J. Perreault, "Muscle short-range stiffness can be used to estimate the endpoint stiffness of the human arm," *J Neurophysiol*, vol. 105, pp. 1633–1641, 2 2011.

[13] G. N. Forman, D. A. Forman, E. J. Avila-Mireles, J. Zenzeri, and M. W. Holmes, "Investigating the Muscular and Kinematic Responses to Sudden Wrist Perturbations During a Dynamic Tracking Task," *Scientific Reports*, vol. 10, 12 2020.